Published in final edited form as:

Nano Lett. 2020 June 10; 20(6): 4073–4083. doi:10.1021/acs.nanolett.9b04877.

Nanoscopic visualization of restricted non-volume cholinergic and monoaminergic transmission with genetically encoded sensors

Paula K. Zhu[1,2,3,11], **W. Sharon Zheng**[4,5], **Peng Zhang**[4], **Miao Jing**[1,6], **Philip M. Borden**[7,12], **Farhan Ali**[8], **Kaiming Guo**[4,9], **Jiesi Feng**[1], **Jonathan S. Marvin**[7], **Yali Wang**[4], **Jinxia Wan**[1], **Li Gan**[10], **Alex C. Kwan**[8], **Li Lin**[9], **Loren L. Looger**[7], **Yulong Li**[1], **Yajun Zhang**[1,4,*]

[1]State Key Laboratory of Membrane Biology and Peking-Tsinghua Center for Life Sciences, Peking University, Beijing 100871, China

[2]Math, Engineering & Science Academy Class of 2020, Albemarle High School, Charlottesville, VA 22901

[3]Summer Secondary School Neurobiology Class of 2019, Harvard University, Cambridge, MA 02138

[4]Department of Pharmacology, University of Virginia School of Medicine, Charlottesville, VA 22908

[5]Department of Biomedical Engineering Class of 2021, University of Virginia School of Medicine, Charlottesville, VA 22908

[6]Chinese Institute for Brain Research, Beijing 100871, China

[7]Janelia Research Campus, Howard Hughes Medical Institute, Ashburn, VA 20147

[8]Department of Psychiatry, Yale University School of Medicine, New Haven, CT 06511

[9]School of Pharmaceutical Sciences, Wenzhou Medical University, Wenzhou 325035, China

[10]Helen and Robert Appel Alzheimer's Disease Research Institute, Weill Cornell Medicine College, New York, NY 10065

[11]Current address: Undergraduate Class of 2024, Harvard College, Cambridge, MA 02138

[12]Current address: LifeEDIT, Research Triangle Park, NC 27709

Abstract

[*]Address for correspondence: Yajun Zhang, Department of Pharmacology, University of Virginia School of Medicine, 1300 Jefferson Park Avenue, Charlottesville, VA 22908, Tel: (434) 243-9562, Fax: (434) 982-3878, yz6k@virginia.edu.

AUTHOR CONTRIBUTIONS: PKZ and YZ conceived the concept and led the project with input from LG, ACK, LL, LLL and YL; PKZ developed MATLAB-based algorithms and analyzed data with assist from WSZ; PZ and YZ performed molecular biology experiments and collected imaging data with assistance from PKZ, KG, FA and YW; LLL, JSM, PMB, YL, JM, JF and JW provided key reagents; PKZ and YZ wrote the manuscript with input from all coauthors.

The authors declare no competing financial interests.

SUPPORTING INFORMATION: Supplementary info available in a single PDF file: Methods; supplementary figures S1 and S2, and supplementary movies S1–4.

How neuromodulatory transmitters diffuse into the extracellular space remains an unsolved fundamental biological question, despite wide acceptance of the volume transmission model. Here, we report development of a method combining genetically encoded fluorescent sensors with high-resolution imaging and analysis algorithms, which permits the first direct visualization of neuromodulatory transm itter diffusion at various neuronal and non-neuronal cells. Our analysis reveals that acetylcholine and monoamines diffuse at individual release sites with a spread length constant of ~0.75 μm. These transmitters employ varied numbers of release sites, and when spatially close-packed release sites co-activate, can spillover into larger subcellular areas. Our data indicate spatially restricted (i.e., non-volume) neuromodulatory transmission to be a prominent intercellular communication mode, reshaping current thinking of control and precision of neuromodulation crucial for understanding behaviors and diseases.

Graphical Abstract

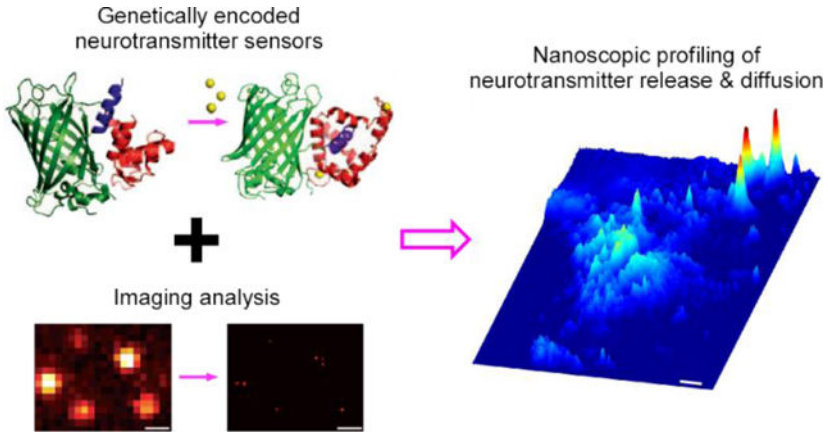

Keywords

Acetylcholine; genetically encode fluorescent sensor; norepinephrine; synaptic transmission; volume transmission

It has been proposed three decades ago that the synaptically released, fast neurotransmitters glutamate and gamma-aminobutyric acid (**GABA**), confined presumably by glial cell barriers, typically mediate one-to-one synaptic transmission, whereas extrasynaptically released neuromodulators, assumed to be less restrained in diffusion and slower in uptake and degradation, mediate one-to-many volume transmission[1, 2]. This theory postulates that the primary mode of intercellular neuromodulatory communication is the volume transmission that takes place among cells in general regions, rather than between specific cells that form direct circuits or contacts. Specifically, this model purports that acetylcholine (**ACh**) and monoamines diffuse into local areas, affecting many different types of nearby cells, with neuropeptides traveling even farther and influencing both local cells and distant cells millimeters away[1, 3]. The volume transmission theory has gained acceptance over time[3, 4], despite lack of supporting evidence and results from multiple combined experimental and simulation studies implicating the contrary[5–9]. Currently, directly examining how endogenous neuromodulatory transmitters diffuse into the extracellular

space under physiological conditions remains a technical challenge, because existing imaging approaches do not allow direct visualization of neuromodulatory transmitter release and diffusion at individual release sites[10, 11].

We developed a method that combines genetically encoded fluorescent neuromodulator sensors[12–18] with imaging and analysis algorithms to evaluate spatial diffusion of endogenously released neuromodulatory transmitters, including ACh and monoamines. This analysis produced the first direct visualization of cholinergic and monoaminergic transmission. High-resolution imaging revealed, among other results, isolated putative release sites presynaptic to neuronal (i.e., medial entorhinal stellate, amygdala, locus coeruleus, lateral geniculate and striatum neurons) and non-neuronal cells (i.e., medial entorhinal astrocytes, pancreatic and adrenal cells). Quantitative analysis yielded cholinergic and monoaminergic transmitter spread length constants of ~0.75 μm, and defined nanoscopic spatial diffusion profiles of these transmitters at both neuronal and non-neuronal cell sites. These results illustrate that, like fast transmitters glutamate and GABA, neuromodulatory transmitters use restricted non-volume transmission as a prominent mode for intercellular communication. These insights into the control and precision of cholinergic and monoaminergic transmission have implications for mechanistic understanding of various behaviors and diseases.

RESULTS

To profile cholinergic transmission, we made Sindbis viral expression of a G protein-coupled receptor-based genetically encoded fluorescent ACh sensor, GACh2.0[12], in layer 2 (**L2**) stellate neurons of the medial entorhinal cortex (**MEC**) in intact mice, and then prepared acute entorhinal slices after ~18 hours of *in vivo* expression (Fig 1A). In acute entorhinal slices, we electrically stimulated MEC L1, that is densely innervated by cholinergic fibers originating from the basal forebrain[19], and measured fluorescence responses (**ΔF/F**) of GACh2.0 expressing neurons. Application of 20 pulses of electrical stimuli at 2 Hz induced robust ΔF/F responses in GACh2.0 expressing neurons (Fig 1B). The ΔF/F responses of fluorescent transmitter sensor expressing cells exhibited a weak correlation with the basal fluorescence F (Fig. S1A–B), suggesting ΔF/F responses to be largely independent of GACh2.0 expression levels (cf.[12]). We developed MATLAB-based signal-processing algorithms to analyze the evoked ΔF/F responses (Fig 1C–D; Methods). The analysis revealed that the evoked ΔF/F responses were restricted to subcellularly isolated areas, frequently forming clusters of individually isolated release sites (Fig 1D; Movie S1). Pixel-wise maximal ΔF/F plots at single isolated release sites revealed the spatial spread of cholinergic responses (Fig 1E). Fitting with a single exponential decay function yielded an ACh spread length constant of ~1.0 μm at entorhinal stellate neurons (Fig 1F). To confirm the cholinergic nature of ΔF/F responses at single release sites, we included atropine, an inhibitor of GACh2.0[12] (and endogenous muscarinic ACh receptors), in the bath solution (Fig 1G). Bath application of atropine largely eliminated ΔF/F responses at single release sites (Fig 1H–I), confirming the spatially restricted fluorescence responses to be cholinergic.

We wished to independently verify the cholinergic nature of the evoked signals at entorhinal stellate neurons. Hence, we expressed a bacterial periplasmic binding protein-based genetically encoded fluorescent ACh sensor, iAChSnFR[13, 14], in L2 entorhinal stellate neurons in intact mice with Sindbis virus, and after ~18 hours of *in vivo* expression, imaged ΔF/F responses in acutely prepared entorhinal slices (Fig 2A). Delivering electrical stimuli at **L**1 elicited ΔF/F responses in iAChSnFR expressing neurons, with clustered isolated release sites seen at subcellular regions (Fig 2B–D; Movie S1). The image results showed that ΔF/F responses were largely independent of iAChSnFR expression levels (Fig. S1C–D). MATLAB-based algorithms revealed the spatially restricted diffusion of ACh after release, fitting well to a single exponential decay function with a spread length constant of ~1.0 μm (Fig 2D–F), identical to the spread length constant determined with GACh2.0. We next imaged iAChSnFR expressing neurons in the amygdala, and found the same spread length constant of ~1.0 μm at amygdalar neurons (Fig 2G), suggesting a general spread length constant for ACh.

To validate the analysis method, we performed control experiments with the 40x objective replaced by a higher magnification (60x) objective, which increased the imaging resolution from ~180 nm/pixel to ~120 nm/pixel. Under these conditions, we again recorded the electrically evoked ΔF/F responses in iAChSnFR expressing entorhinal stellate neurons, yielding a similar ACh spread length constant of ~1.1 μm (Fig 2H–K; Movie S3). The results rule out potential artifacts that might be introduced during imaging analysis and reconstruction[20]. As a control, we analyzed ΔF/F responses and basal fluorescence F and found only a weak correlation between them (Fig. S1E–F), suggesting ΔF/F responses to be largely independent of iAChSnFR expression levels. Bath application of tetrodotoxin (TTX), which blocks action potential-evoked synaptic release, diminished the evoked ΔF/F responses in iAChSnFR expressing entorhinal stellate neurons (Fig 2I, 2L). Moreover, application of 0 Ca^{2+}/10 mM Mg^{2+} bath solution, which suppresses all synaptic activities[21], abolished the evoked ΔF/F responses in iAChSnFR expressing entorhinal stellate neurons (Fig 2L), confirming the synaptic origin of signals (cf.[14]). Together, these results indicate that restricted transmission is a common feature of cholinergic signaling on neurons.

We then investigated ACh signals at astrocytes, which express high levels of muscarinic ACh receptors in their fine distal processes involved in tripartite synapses[22]. We used a lentiviral vector carrying a glial fibrillary acidic protein (**GFAP**) promoter to achieve targeted expression of iAChSnFR in entorhinal astrocytes in mice *in vivo* for ~7 days, and then imaged electrically evoked ΔF/F responses *ex vivo* in acute entorhinal brain slices (Fig 3A). Electric stimuli evoked robust ΔF/F responses in iAChSnFR expressing astrocytes, and individual, isolated release sites with large ΔF/F responses were often observed at distal astrocytic processes (Fig 3B–C), illustrating potent cholinergic transmission at astrocytic areas with the highest muscarinic ACh receptor expression[22]. ACh released at these individual sites also had an ACh spread length constant of ~1.0 μm (Fig 3C–E). Together, these results suggest similarly restricted cholinergic transmission for intercellular communication at both neurons and astrocytes.

We then investigated cholinergic transmission at the pancreas and adrenal gland, in which parasympathetic nerve terminals release ACh to control insulin secretion, and to regulate

blood pressure and steroid release, respectively[23, 24]. We induced Sindbis viral expression of GACh2.0 in the mouse pancreas and adrenal gland *in vivo,* and imaged fluorescence responses of GACh2.0 expressing cells in acute pancreatic and adrenal slices after 18 hours expression (Fig 3F). Electrical stimulation of local parasympathetic cholinergic fibers evoked ΔF/F responses in GACh2.0 expressing pancreatic and adrenal cells (Fig 3G–H), confirming our previous report[12]. As with neurons and astrocytes, evoked ΔF/F responses exhibited clusters of isolated individual release sites at GACh2.0 expressing cells (Fig 3H), and analysis of transmitter diffusion at these release sites gave a spread length constant of ~1.1 μm at pancreatic and adrenal cells (Fig 3H–J). Collectively, these data showed no differences in ACh spread length constants at neuronal and non-neuronal cells measured with GACh2.0 and iAChSnFR sensors at high resolutions (~120 nm/pixel and ~180 nm/pixel) (Fig 3K), supporting the generalization of restricted cholinergic transmission as a major intercellular communication mode for various cell types.

We next examined adrenergic transmission using a genetically encoded fluorescent sensor for norepinephrine (NE), $GRAB_{NE1m}$[15]. We employed Sindbis virus for *in vivo* expression of $GRAB_{NE1m}$ in the mouse amygdala, that is heavily innervated by noradrenergic fibers from the locus coeruleus[25]. Approximately 18 hours later, we prepared acute amygdalar slices, locally delivered 20 pulses of 4-Hz electrical stimuli, and imaged fluorescence responses of $GRAB_{NE1m}$ expressing neurons (Fig 4A). Electric stimuli evoked slow ΔF/F responses, typically covering the entire somatic areas of $GRAB_{NE1m}$ expressing amygdalar neurons, although individual isolated release sites were occasionally seen (Fig 4B–D; Movie S4). ΔF/F responses had only a weak correlation with the basal fluorescence F, suggesting the responses to be largely independent of GRABNE1m expression levels (Fig. S1G–H). Spatial diffusion analysis of ΔF/F responses at isolated single release sites produced an NE spread length constant of ~1.2 μm at amygdalar neurons (Fig 4D–F), similar in size to spatially restricted postsynaptic adrenergic receptor expression hot spots[26]. To confirm the findings, we imaged $GRAB_{NE1m}$ expressing neurons in the locus coeruleus, and found an NE spread length constant of ~0.9 μm at coerulear neurons (Fig 4G), suggesting a general spread length constant of ~1.0 μm for NE at different cell types.

Finally, we used the same *in vivo* Sindbis viral expression in the lateral geniculate nucleus and striatum, and subsequent *ex vivo* thalamic and striatal brain slice preparations, to characterize the spatial profiles of two other monoamine transmitters, serotonin (**5HT**) and dopamine (**DA**), with genetically encoded fluorescent 5HT and DA sensors, respectively[16–18]. Our analysis of electrically evoked ΔF/F responses showed that 5HT at geniculate neurons and DA at striatal neurons had the same spread length constant of ~1.0 μm (Fig 4G). These data are consistent with the idea of restricted non-volume monoaminergic transmission as a major intercellular communication mode for various neuromodulatory transmitters at different cell types.

To correct for microscopic point-spread function diffraction effects in recorded images, we obtained our microscopic point-spread functions with 23 nm green GATTA beads under both 40x and 60x objectives (Fig 5A–E). Deconvolution based on the measured point-spread functions yielded the true spread length constants of 0.74±0.03 μm (n=10 transmitters at various cells) (Fig 5F), indicating ~35% overestimation before diffraction correction.

DISCUSSION

In this study, we have developed an imaging and analysis method that permits the first visualization of release and diffusion of endogenous neuromodulatory transmitters and determination of nanoscopic spatial diffusion profiles of these transmitters. These results suggest that highly restricted, non-volume neuromodulatory transmission is a key mode for intercellular communication between cells in neuronal and non-neuronal tissues; the fine control and precision of cholinergic and monoaminergic signals are likely to be essential for understanding various neuromodulation-mediated behaviors and diseases.

Restricted vs. volume transmission

Visualization of highly restricted cholinergic and monoaminergic transmission directly challenges the prevailing theory of volume transmission of neuromodulators. The volume transmission theory proposes that neuromodulatory transmitters readily diffuse over long distances and affect many different types of nearby cells (in the case of ACh and monoamines) and distant cells millimeters away (in the case of neuropeptides)[1, 3]. Three decades later, volume transmission remains the dominant theory for neuromodulatory transmission[3, 4]. However, the theory is based primarily on the notion that endogenously released neuromodulatory transmitters might behave similarly as exogenously applied ones (that diffuse more freely in the extrasynaptic space), an assumption that has not yet been corroborated by any direct experimental evidence[8, 9].

Over the years, researchers have strived to gauge neurotransmitter diffusion in more quantitative ways. Although previous imaging techniques do not permit direct visualization of endogenous transmitter release and diffusion at individual release sites[10, 11], early studies ingeniously utilized mathematical models to simulate evoked neuromodulatory releases, yielding excellent estimations of transmitter spread areas of ~5.0–10.0 μm in diameter[5–7]. However, these studies were underappreciated, due presumably to indirect calculation approaches and/or dependence on simulation assumptions. Here, combining super-resolution microscopic analysis strategies[27, 28] and genetically-encoded sensors[12–18], we directly visualized and precisely measured diffusion spread length constants of ~0.75 μm for both ACh and monoamines, accounting roughly for the previously reported diffusion areas estimated from both single isolated and multiple closely clustered release sites[5–7]. These findings support restricted non-volume neuromodulatory transmission.

Implications in physiology

Our diffusion spread constants specify peak neuromodulatory transmitter concentrations to drop by ~98% at 5 μm away from the release sites. Because many genetically encoded neuromodulatory transmitter sensors have affinities comparable to their primogenitors, or endogenous transmitter receptors[12–18], neuromodulatory transmitters released at single sites might induce negligible fluorescent signals and minimal postsynaptic effects in distal areas of the same cells, but not neighboring cells (~15–50 μm away on average) expressing even high-affinity receptors (e.g., m_2 muscarinic receptors[29]). Indeed, attention-engaging visual stimulation typically induces reliable ACh release at a few sparse visual cortical neurons, but not their neighbors, in awake mice[12], providing *in vivo* experimental support. Interestingly,

neuromodulatory release sites frequently form well-ordered clusters, mirroring presynaptic neuromodulatory bouton organization[30], which may be important for super-linear signal summation[31], signal plasticity[32, 33], and/or fine-tuning of intercellular signals[34]. Obviously, as with the fast transmitters glutamate (e.g., via NMDA receptors[35]) and GABA (e.g., via δ subunit-containing $GABA_A$ receptors[36]), neuromodulatory transmitters may employ high affinity receptors[29, 37] and/or large clusters of release sites (Fig 4C–D) to achieve certain volume transmission effects under physiological and pathological conditions[8, 9, 14, 38, 39]. Importantly, neuromodulatory transmitter-releasing neurons routinely fire low-frequency action potentials of ~0.02–8 Hz (with average firing rates <<1 Hz) in intact animals[40–44], and they release transmitters with low release probabilities and/or strong depression (our unpublished data), indicating that under many physiological conditions, neuromodulatory transmitter release is sparse and low-level. These results suggest that highly restricted transmission with subcellular signal precision is an important mode of neuromodulatory transmission.

Nanoscale pre-post synaptic organization is a fundamental determinant of transmission signal amplitude and reliability, and across various synapses, the amount of released transmitters, width of synaptic clefts, and location of postsynaptic transmitter receptors all seem to be optimized to maximize synaptic efficacy[45–47]. Here, our visualized spatial diffusion analysis reveals spread length constants of ~0.75 μm for ACh (released synaptically and extrasynaptically[37]) and monoamines at various cell types. Interestingly, the same analysis made on evoked ΔF/F responses at iGluSnFR[48] expressing amygdalar neurons yields a spread length constant of ~0.62 um for glutamate (unpublished data; see also[49]), a slightly smaller value expected for the negatively charged glutamate that can be electrophoretically influenced by excitatory currents[50]. Moreover, we see the same diffusion spread length constant for an endogenously released neuropeptide using a genetically encoded neuropeptide sensor (unpublished data). The similar spread length constants observed across various cell types for fast (e.g., glutamate) and slow transmitters (e.g., ACh, monoamines and neuropeptide) raises the interesting possibility that transmitter diffusion is optimized across various synapses for transmission efficacy and precision. These results formulate a general concept that both fast (i.e., glutamate and GABA) and neuromodulatory transmitters utilize highly restricted transmission as a key mode of intercellular communication, with complementation provided by volume transmission under certain conditions.

Implications in diseases

Highly restricted, non-volume neuromodulatory transmission explains some perplexing clinical observations and suggests new potential therapeutic interventions. For example, dysregulation of cholinergic transmission is seen in many neurological disorders, including Alzheimer's disease. In fact, the only available therapy for Alzheimer's disease is based on the finding of diminishing ACh release and deteriorating cholinergic neurons in Alzheimer's brains — the cholinergic hypothesis[51]. Currently, all FDA-approved Alzheimer's drugs directly or indirectly inhibit acetylcholinesterase to boost cholinergic signals. These medicines have limited efficacy in cognitive improvement, and upon medication termination, induce irreversible, accelerated deterioration[52, 53]. Our new findings can account for these

clinical observations since: 1) acetylcholinesterase inhibitors could reduce physiological precision of cholinergic transmission (cf.[8, 9]), explaining the only modest cognitive improvement; and 2) long-term application of acetylcholinesterase inhibitors could homeostatically up-regulate acetylcholinesterase levels in Alzheimer's patients and/or down-regulate presynaptic ACh release[53], explaining the accelerated deterioration upon medication termination. Similarly, impaired adrenergic transmission often appears as the first pathological correlate of cognitive decline in Alzheimer's disease[54, 55]. Our results underscore contributions of fine-tuned adrenergic transmission to molding of wakefulness and attention[34], optimization of behavior in complex social and physical environments[56, 57], and impairment of complex mental tasks (e.g., reasoning and abstract thinking) in Alzheimer's patients[58]. The new insights into cholinergic and adrenergic transmission immediately suggest multiple regulatory mechanisms as potentially effective intervention targets and set the physiological transmission baseline for future medication testing and development.

Dysregulation of central cholinergic and monoaminergic transmission is also linked to other major brain disorders, including addiction[59, 60], autism[61], epilepsy[62, 63], Parkinson's disease[64, 65], and sleep disorders[57], as well as a large group of anxiety and mood disorders[66–68]. Moreover, defective cholinergic and monoaminergic signals may underlie pathogenesis of a number of non-neurological diseases, including cardiovascular disease, diabetes, immune deficiency and tumorigenesis[69–73]. We expect our new method to lead to more comprehensive understanding of fundamental properties and regulation of cholinergic and monoaminergic transmission, which is essential for dissecting pathogenic mechanisms and developing effective interventions for these diseases.

Supplementary Material

Refer to Web version on PubMed Central for supplementary material.

ACKNOWLEDGEMENTS:

We thank members of the Julius Zhu lab for suggestions and technical support, and Drs. Gerard Borst, Yiyang Gong, Ling-Gang Wu and Zhuan Zhou for inspirational discussions and critical comments. This study is supported in part by Intel International Science and Engineering Fair Award (PKZ), Harrison Undergraduate Research Award (WSZ), Alzheimer's Association Postdoc-to-Faculty Transitioning Research Fellowships AARF-17-504924 (FA) and AARF-19-619387 (PZ), National Natural Science Foundation of China Young Scholar Award NSFC81701070 (YW), and a Peking-Tsinghua Center Excellence Postdoctoral Fellowship (YZ).

REFERENCES:

1. Agnati LF; Bjelke B; Fuxe K Volume transmission in the brain. Am Sci 1992, 80, (4), 362–373.
2. Zoli M; Jansson A; Sykova E; Agnati LF; Fuxe K Volume transmission in the CNS and its relevance for neuropsychopharmacology. Trends in pharmacological sciences 1999, 20, (4), 142–50. [PubMed: 10322499]
3. Borroto-Escuela DO; Perez De La Mora M; Manger P; Narvaez M; Beggiato S; Crespo-Ramirez M; Navarro G; Wydra K; Diaz-Cabiale Z; Rivera A; Ferraro L; Tanganelli S; Filip M; Franco R; Fuxe K Brain dopamine transmission in health and Parkinson's disease: modulation of synaptic transmission and olasticity through volume transmission and dopamine heteroreceptors. Front Synaptic Neurosci 2018, 10, 20. [PubMed: 30042672]

4. Gundersen V; Storm-Mathisen J; Bergersen LH Neuroglial transmission. Physiological reviews 2015, 95, (3), 695–726. [PubMed: 26084688]
5. Beckstead MJ; Grandy DK; Wickman K; Williams J T Vesicular dopamine release elicits an inhibitory postsynaptic current in midbrain dopamine neurons. Neuron 2004, 42, (6), 939–46. [PubMed: 15207238]
6. Courtney NA; Ford CP The timing of dopamine- and noradrenaline-mediated transmission reflects underlying differences in the extent of spillover and pooling. J Neurosci 2014, 34, (22), 7645–56. [PubMed: 24872568]
7. Courtney NA; Ford CP Mechanisms of 5-HT1A receptor-mediated transmission in dorsal raphe serotonin neurons. The Journal of physiology 2016, 594, (4), 953–65. [PubMed: 26634643]
8. Barbour B; Hausser M Intersynaptic diffusion of neurotransmitter. Trends in neurosciences 1997, 20, (9), 377–84. [PubMed: 9292962]
9. Sarter M; Parikh V; Howe WM Phasic acetylcholine release and the volume transmission hypothesis: time to move on. *Nature reviews*. Neuroscience 2009, 10, (5), 383–90. [PubMed: 19377503]
10. Sykova E; Nicholson C Diffusion in brain extracellular space. Physiological reviews 2008, 88, (4), 1277–340. [PubMed: 18923183]
11. Zheng K; Jensen TP; Savtchenko LP; Levitt JA; Suhling K; Rusakov DA Nanoscale diffusion in the synaptic cleft and beyond measured with time-resolved fluorescence anisotropy imaging. Sci Rep 2017, 7, 42022. [PubMed: 28181535]
12. Jing M; Zhang P; Wang G; Feng J; Mesik L; Zeng J; Jiang H; Wang S; Looby JC; Guagliardo NA; Langma LW; Lu J; Zuo Y; Talmage DA; Role LW; Barrett PQ; Zhang LI; Luo M; Song Y; Zhu JJ; Li Y A genetically encoded fluorescent acetylcholine indicator for in vitro and in vivo studies. Nature biotechnology 2018, 36, (8), 726–737.
13. Kazemipour A; Novak O; Flickinger D; Marvin JS; Abdelfattah AS; King J; Borden PM; Kim JJ; Al-Abdullatif SH; Deal PE; Miller EW; Schreiter ER; Druckmann S; Svoboda K; Looger LL; Podgorski K Kilohertz frame-rate two-photon tomography. Nature methods 2019, 16, (8), 778–786. [PubMed: 31363222]
14. Borden PM; Zhang P; Shivange AV; Marvin JS; Cichon J; Dan C; Podgorski K; Figueiredo A; Novak O; Tanimoto M; Shigetomi E; Lobas MA; Kim H; Zhu PK; Zhang Y; Zheng WS; Fan C-C; Wang W; Xiang B; Gan L; Zhang G-X; Guo K; Lin L; Cai Y; Yee AG; Aggarwal A; Ford CP; Rees DC; Dietrich D; Khakh BS; Dittman JS; Gan W-B; Koyama M; Jayaraman V; Cheer JF; Lester HA; Zhu JJ; Looger LL A fast genetically encoded fluorescent sensor for faithful in vivo acetylcholine detection in mice, fish, worms and flies. bioRxiv 2 8, 2020, doi: 10.1101/2020.02.07.939504, under review in Cell.
15. Feng J; Zhang C; Lischinsky JE; Jing M; Zhou J; Wang H; Zhang Y; Dong A; Wu Z; Wu H; Chen W; Zhang P; Zou J; Hires SA; Zhu JJ; Cui G; Lin D; Du J; Li Y A genetically encoded fluorescent sensor for rapid and specific in vivo detection of norepinephrine. Neuron 2019, 102, (4), 745–761 e8. [PubMed: 30922875]
16. Wan J; Peng W; Li X; Qian T; Song K; Zeng J; Deng F; Hao S; Feng J; Zhang P; Zhang Y; Zou J; Pan S; Zhu JJ; Jing M; Xu M; Li Y A genetically encoded GRAB sensor for measuring serotonin dynamics in vivo. bioRxiv 2 24, 2020, 10.1101/2020.02.24.962282, under review in Nature Neuroscience.
17. Patriarchi T; Cho JR; Merten K; Howe MW; Marley A; Xiong WH; Folk RW; Broussard GJ; Liang RQ; Jang MJ; Zhong HN; Dombeck D; von Zastrow M; Nimmerjahn A; Gradinaru V; Williams JT; Tian L Ultrafast neuronal imaging of dopamine dynamics with designed genetically encoded sensors. Science 2018, 360, (6396), 1420-+.
18. Sun FM; Zeng JZ; Jing M; Zhou JH; Feng JS; Owen SF; Luo YC; Li FN; Wang H; Yamaguchi T; Yong ZH; Gao YJ; Peng WL; Wang LZ; Zhang SY; Du JL; Lin DY; Xu M; Kreitzer AC; Cui GH; Li YL A genetically encoded fluorescent sensor enables rapid and specific detection of dopamine in flies, fish, and mice. Cell 2018, 174, (2), 481–96. [PubMed: 30007419]
19. Ray S; Naumann R; Burgalossi A; Tang Q; Schmidt H; Brecht M Grid-layout and theta-modulation of layer 2 pyramidal neurons in medial entorhinal cortex. Science 2014, 343, (6173), 891–6. [PubMed: 24457213]

20. Small A; Stahlheber S Fluorophore localization algorithms for super-resolution microscopy. Nature methods 2014, 11, (3), 267–79. [PubMed: 24577277]
21. McCormack SG; Stornetta RL; Zhu JJ Synaptic AMPA receptor exchange maintains bidirectional plasticity. Neuron 2006, 50, (1), 75–88. [PubMed: 16600857]
22. Van Der Zee EA; De Jong GI; Strosberg AD; Luiten PG Muscarinic acetylcholine receptor-expression in astrocytes in the cortex of young and aged rats. Glia 1993, 8, (1), 42–50. [PubMed: 8509163]
23. Satin LS; Kinard TA Neurotransmitters and their receptors in the islets of Langerhans of the pancreas: what messages do acetylcholine, glutamate, and GABA transmit? Endocrine 1998, 8, (3), 213–23. [PubMed: 9741825]
24. Ungar A; Phillips JH Regulation of the adrenal medulla. Physiological reviews 1983, 63, (3), 787–843. [PubMed: 6308693]
25. Foote SL; Bloom FE; Astonjones G Nucleus locus ceruleus - new evidence of anatomical and physiological specificity. Physiological reviews 1983, 63, (3), 844–914. [PubMed: 6308694]
26. Sungkaworn T; Jobin ML; Burnecki K; Weron A; Lohse MJ; Calebiro D Single-molecule imaging reveals receptor-G protein interactions at cell surface hot spots. Nature 2017, 550, (7677), 543–547. [PubMed: 29045395]
27. Sauer M Localization microscopy coming of age: from concepts to biological impact. Journal of cell science 2013, 126, (Pt 16), 3505–13. [PubMed: 23950110]
28. Li H; Vaughan JC Switchable fluorophores for single-molecule localization microscopy. Chemical reviews 2018, 118, (18), 9412–9454. [PubMed: 30221931]
29. Kellar KJ; Martino AM; Hall DP Jr.; Schwartz RD; Taylor RL High-affinity binding of [3H]acetylcholine to muscarinic cholinergic receptors. J Neurosci 1985, 5, (6), 1577–82. [PubMed: 4009247]
30. Liu C; Kershberg L; Wang J; Schneeberger S; Kaeser PS Dopamine secretion is mediated by sparse active zone-like release sites. Cell 2018, 172, (4), 706–718 e15. [PubMed: 29398114]
31. Larkum ME; Nevian T Synaptic clustering by dendritic signalling mechanisms. Current opinion in neurobiology 2008, 18, (3), 321–31. [PubMed: 18804167]
32. Makino H; Malinow R Compartmentalized versus global synaptic plasticity on dendrites controlled by experience. Neuron 2011, 72, (6), 1001–11. [PubMed: 22196335]
33. Fu M; Yu X; Lu J; Zuo Y Repetitive motor learning induces coordinated formation of clustered dendritic spines in vivo. Nature 2012, 483, (7387), 92–5. [PubMed: 22343892]
34. Carter ME; Yizhar O; Chikahisa S; Nguyen H; Adamantidis A; Nishino S; Deisseroth K; de Lecea L Tuning arousal with optogenetic modulation of locus coeruleus neurons. Nature neuroscience 2010, 13, (12), 1526–33. [PubMed: 21037585]
35. Rusakov DA; Kullmann DM; Stewart MG Hippocampal synapses: do they talk to their neighbours? Trends in neurosciences 1999, 22, (9), 382–8. [PubMed: 10441295]
36. Brickley SG; Mody I Extrasynaptic GABA**a** receptors: their function in the CNS and implications for disease. Neuron 2012, 73, (1), 23–34. [PubMed: 22243744]
37. Dani JA; Bertrand D Nicotinic acetylcholine receptors and nicotinic cholinergic mechanisms of the central nervous system. Annual review of pharmacology and toxicology 2007, 47, 699–729.
38. Seamans JK; Yang CR The principal features and mechanisms of dopamine modulation in the prefrontal cortex. Progress in neurobiology 2004, 74, (1), 1–58. [PubMed: 15381316]
39. Okaty BW; Commons KG; Dymecki SM Embracing diversity in the 5-HT neuronal system. Nature reviews. Neuroscience 2019, 20, (7), 397–424. [PubMed: 30948838]
40. Simon AP; Poindessous-Jazat F; Dutar P; Epelbaum J; Bassant MH Firing properties of anatomically identified neurons in the medial septum of anesthetized and unanesthetized restrained rats. J Neurosci 2006, 26, (35), 9038–46. [PubMed: 16943562]
41. Duque A; Tepper JM; Detari L; Ascoli GA; Zaborszky L Morphological characterization of electrophysiologically and immunohistochemically identified basal forebrain cholinergic and neuropeptide Y-containing neurons. Brain structure & function 2007, 212, (1), 55–73. [PubMed: 17717698]

42. Aston-Jones G; Bloom FE Activity of norepinephrine-containing locus coeruleus neurons in behaving rats anticipates fluctuations in the sleep-waking cycle. J Neurosci 1981, 1, (8), 876–86. [PubMed: 7346592]
43. Cohen JY; Amoroso MW; Uchida N Serotonergic neurons signal reward and punishment on multiple timescales. eLife 2015, 4, e06346 DOI: 10.7554/eLife.06346.
44. Grace AA; Bunney BS The control of firing pattern in nigral dopamine neurons: single spike firing. J Neurosci 1984, 4, (11), 2866–76. [PubMed: 6150070]
45. Savtchenko LP; Sylantyev S; Rusakov DA Central synapses release a resource-efficient amount of glutamate. Nature neuroscience 2013, 16, (1), 10–2. [PubMed: 23242311]
46. Savtchenko LP; Rusakov DA The optimal height of the synaptic cleft. Proceedings of the National Academy of Sciences of the United States of America 2007, 104, (6), 1823–8. [PubMed: 17261811]
47. Haas KT; Compans B; Letellier M; Bartol TM; Grillo-Bosch D; Sejnowski TJ; Sainlos M; Choquet D; Thoumine O; Hosy E Pre-post synaptic alignment through neuroligin-1 tunes synaptic transmission efficiency. eLife 2018, 7, e31755 DOI: 10.7554/eLife.31755. [PubMed: 30044218]
48. Marvin JS; Borghuis BG; Tian L; Cichon J; Harnett MT; Akerboom J; Gordus A; Renninger SL; Chen TW; Bargmann CI; Orger MB; Schreiter ER; Demb JB; Gan WB; Hires SA; Looger LL An optimized fluorescent probe for visualizing glutamate neurotransmission. Nature methods 2013, 10, (2), 162–70. [PubMed: 23314171]
49. Jensen TP; Zheng K; Cole N; Marvin JS; Looger LL; Rusakov DA Multiplex imaging relates quantal glutamate release to presynaptic Ca2+ homeostasis at multiple synapses in situ. Nature communications 2019, 10, (1), 1414.
50. Sylantyev S; Savtchenko LP; Niu YP; Ivanov AI; Jensen TP; Kullmann DM; Xiao MY; Rusakov DA Electric fields due to synaptic currents sharpen excitatory transmission. Science 2008, 319, (5871), 1845–9. [PubMed: 18369150]
51. Mash DC; Flynn DD; Potter LT Loss of M2 muscarine receptors in the cerebral cortex in Alzheimer's disease and experimental cholinergic denervation. Science 1985, 228, (4703), 1115–7. [PubMed: 3992249]
52. Zemek F; Drtinova L; Nepovimova E; Sepsova V; Korabecny J; Klimes J; Kuca K Outcomes of Alzheimer's disease therapy with acetylcholinesterase inhibitors and memantine. Expert opinion on drug safety 2014, 13, (6), 759–74. [PubMed: 24845946]
53. Ashford JW Treatment of Alzheimer's disease: the legacy of the cholinergic hypothesis, neuroplasticity, and future directions. Journal of Alzheimer's disease : JAD 2015, 47, (1), 149–56. [PubMed: 26402763]
54. Simic G; Leko MB; Wray S; Harrington CR; Delalle I; Jovanov-Milosevic N; Bazadona D; Buee L; de Silva R; Di Giovanni G; Wischik CM; Hof PR Monoaminergic neuropathology in Alzheimer's disease. Progress in neurobiology 2017, 151, 101–138. [PubMed: 27084356]
55. Mather M; Harley CW The locus coeruleus: essential for maintaining cognitive function and the aging brain. Trends Cogn Sci 2016, 20, (3), 214–226. [PubMed: 26895736]
56. Aston-Jones G; Cohen JD An integrative theory of locus coeruleus-norepinephrine function: Adaptive gain and optimal performance. Annual review of neuroscience 2005, 28, 403–450.
57. Scammell TE; Arrigoni E; Lipton JO Neural circuitry of wakefulness and sleep. Neuron 2017, 93, (4), 747–765. [PubMed: 28231463]
58. McKhann GM; Knopman DS; Chertkow H; Hyman BT; Jack CR Jr.; Kawas CH; Klunk WE; Koroshetz WJ; Manly JJ; Mayeux R; Mohs RC; Morris JC; Rossor MN; Scheltens P; Carrillo MC; Thies B; Weintraub S; Phelps CH The diagnosis of dementia due to Alzheimer's disease: recommendations from the National Institute on Aging-Alzheimer's Association workgroups on diagnostic guidelines for Alzheimer's disease. Alzheimer's & dementia : the journal of the Alzheimer's Association 2011, 7, (3), 263–9.
59. Williams MJ; Adinoff B The role of acetylcholine in cocaine addiction. Neuropsychopharmacology : official publication of the American College of Neuropsychopharmacology 2008, 33, (8), 1779–97. [PubMed: 17928814]
60. Grace AA Dysregulation of the dopamine system in the pathophysiology of schizophrenia and depression. Nature reviews. Neuroscience 2016, 17, (8), 524–32. [PubMed: 27256556]

61. Bast N; Poustka L; Freitag CM The locus coeruleus-norepinephrine system as pacemaker of attention - a developmental mechanism of derailed attentional function in autism spectrum disorder. European Journal of Neuroscience 2018, 47, (2), 115–125. [PubMed: 29247487]

62. Giorgi FS; Pizzanelli C; Biagioni F; Murri L; Fornai F The role of norepinephrine in epilepsy: from the bench to the bedside. Neuroscience and biobehavioral reviews 2004, 28, (5), 507–24. [PubMed: 15465138]

63. Platt B; Riedel G The cholinergic system, EEG and sleep. Behavioural brain research 2011, 221, (2), 499–504. [PubMed: 21238497]

64. Ballinger EC; Ananth M; Talmage DA; Role LW Basal forebrain cholinergic circuits and signaling in cognition and cognitive decline. Neuron 2016, 91, (6), 1199–218. [PubMed: 27657448]

65. Weinshenker D Long road to ruin: noradrenergic dysfunction in neurodegenerative disease. Trends in neurosciences 2018, 41, (4), 211–223. [PubMed: 29475564]

66. Ravindran LN; Stein MB The pharmacologic treatment of anxiety disorders: a review of progress. The Journal of clinical psychiatry 2010, 71, (7), 839–54. [PubMed: 20667290]

67. Higley MJ; Picciotto MR Neuromodulation by acetylcholine: examples from schizophrenia and depression. Current opinion in neurobiology 2014, 29, 88–95. [PubMed: 24983212]

68. Gold PW The organization of the stress system and its dysregulation in depressive illness. Molecular psychiatry 2015, 20, (1), 32–47. [PubMed: 25486982]

69. Kruse AC; Kobilka BK; Gautam D; Sexton PM; Christopoulos A; Wess J Muscarinic acetylcholine receptors: novel opportunities for drug development. Nature reviews. Drug discovery 2014, 13, (7), 549–60. [PubMed: 24903776]

70. Soreq H Checks and balances on cholinergic signaling in brain and body function. Trends in neurosciences 2015, 38, (7), 448–58. [PubMed: 26100140]

71. Wood SK; Valentino RJ The brain norepinephrine system, stress and cardiovascular vulnerability. Neuroscience and biobehavioral reviews 2017, 74, 393–400. [PubMed: 27131968]

72. Dantzer R Neuroimmune interactions: from the brain to the immune system and vice versa. Physiological reviews 2018, 98, (1), 477–504. [PubMed: 29351513]

73. Berger M; Gray JA; Roth BL The expanded biology of serotonin. Annual review of medicine 2009, 60, 355–66.

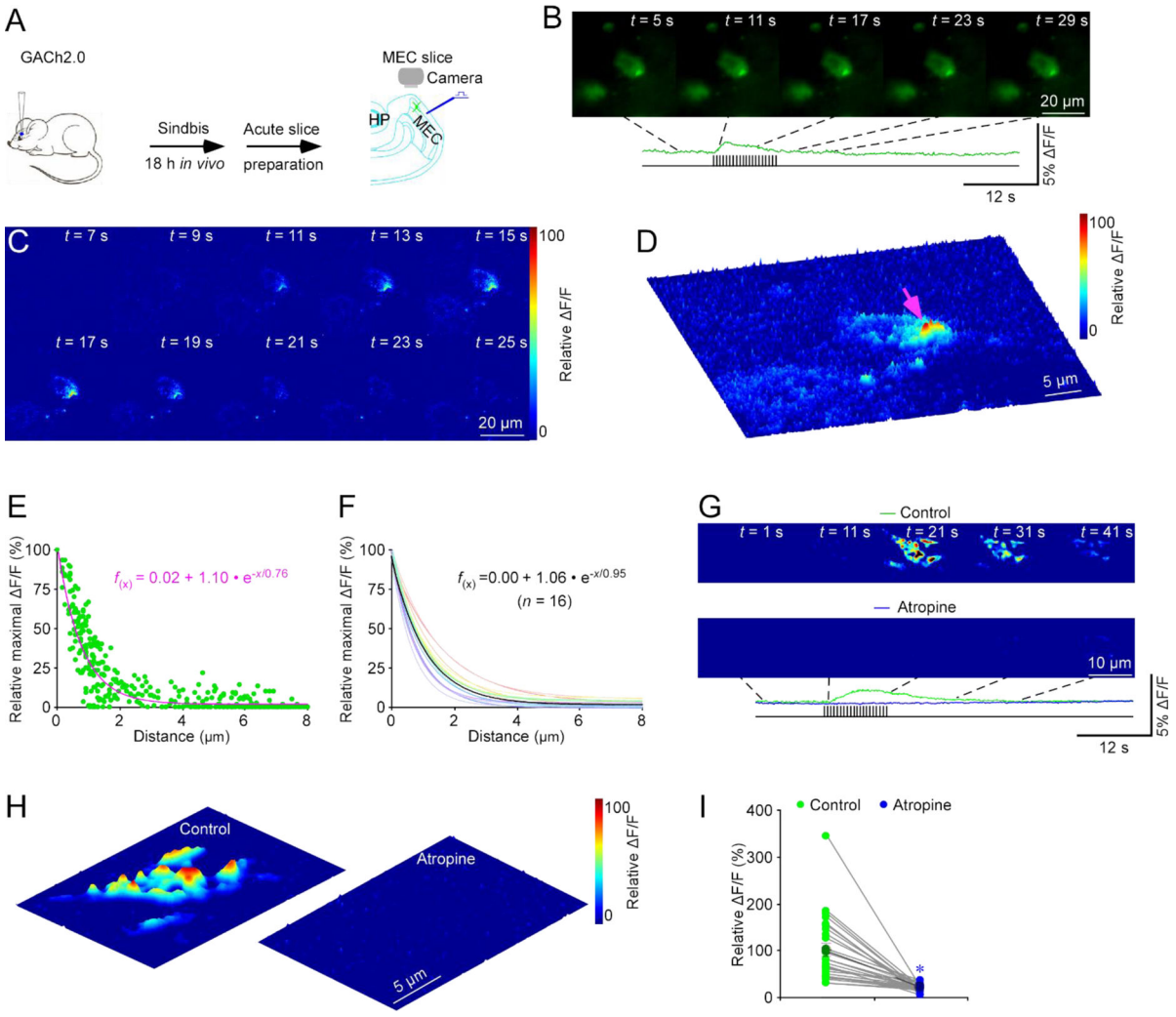

Figure 1. GACh2.0 spatiotemporally profiles cholinergic transmission at MEC stellate neurons.

(**A**) Schematic drawing of the design of stimulation-imaging experiments in acute mouse MEC slices. HP: Hippocampus; MEC: Medial entorhinal cortex.

(**B-D**) Snapshots of fluorescence ΔF/F responses (**B**), heatmap displays of time-dependent spatial ΔF/F responses (**C**) and three-dimensional spatiotemporal ΔF/F profiling (**D**) of a GACh2.0 expressing entorhinal stellate cell in response to local electrical stimuli. Note one isolated release site indicated by pink arrow in **D**.

(**E**) Plot of relative maximal ΔF/F of each pixel against its distance to the pixel with largest maximum ΔF/F at the isolated release site indicated by pink arrow in **D**. Fitting the data points in this plot with a single exponential decay function (pink line) yields an estimated ACh spread length constant of 0.76 μm.

(**F**) Summary plot of volume spread length constants obtained from putative single release sites and the average volume spread length constant of 0.95±0.07 μm for cholinergic transmission at entorhinal stellate neurons (n = 16 from 6 neurons from 5 animals). Note the average single exponential decay function fitting curve in black.

(**G**) Heatmap snapshots of time-dependent spatial ΔF/F responses of a GACh2.0 expressing entorhinal stellate neuron in response to local electrical stimuli in the normal bath solution and bath solution containing 10 μM atropine.
(**H**) Heatmap displays of three-dimensional spatiotemporal ΔF/F profiling of the same GACh2.0 expressing entorhinal stellate neuron in response to local electrical stimuli in the normal bath solution and bath solution containing atropine.
(**I**) Values of peak ΔF/F responses of putative single release sites measured in the normal bath solution and bath solution containing atropine (Control: 100.0±13.1%; Atropine: 21.5±1.5%; $n = 27$ from 6 neurons from 6 animals; $Z = -4.541$, $p < 0.005$). Large gray dots indicate average responses and asterisk indicates $p < 0.05$ (Wilcoxon Rank Sum test).

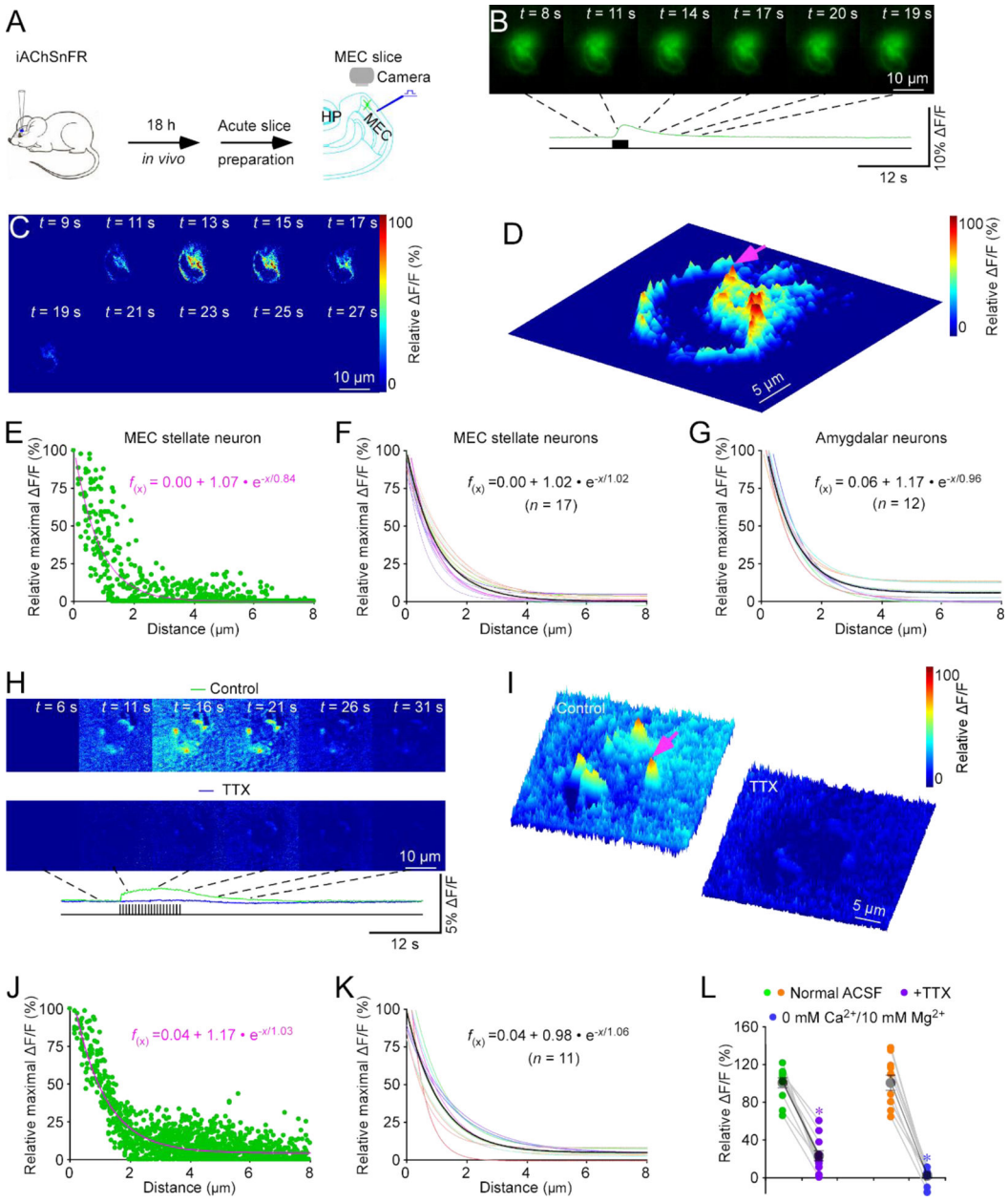

Figure 2. iAChSnFR spatiotemporally profiles cholinergic transmission at MEC stellate cell.

(**A**) Schematic drawing of the design of stimulation-imaging experiments in acute mouse MEC slices. HP: Hippocampus; MEC: Medial entorhinal cortex.

(**B-D**) Snapshots of fluorescence ΔF/F responses (**B**), heatmap displays of time-dependent spatial ΔF/F responses (**C**) and three-dimensional spatiotemporal ΔF/F profiling (**D**) of an iAChSnFR expressing entorhinal stellate neuron in response to local electrical stimuli. Note fluorescence ΔF/F responses imaged at ~180 nm/pixel resolution (with 40x objective) in **B-D** and one isolated release site indicated by pink arrow in **D**.

(**E**) Plot of relative maximal ΔF/F of each pixel against its distance to the pixel with largest maximal ΔF/F at the isolated release site indicated by pink arrow in **D**. Fitting the data

points in this plot with a single exponential decay function (pink line) yields an estimated ACh spread length constant of 1.02 μm.

(**F**) Summary plot of volume spread length constants obtained from putative single release sites and the average volume spread length constant of 1.02±0.05 μm for cholinergic transmission at entorhinal stellate neurons (n = 17 from 8 neurons from 8 animals). Note the average single exponential decay function fitting curve in black.

(**G**) Summary plot of volume spread length constants obtained from putative single release sites and the average ACh spread length constant of 0.96±0.02 μm for cholinergic transmission at amygdalar neurons (n = 12 from 4 neurons from 4 animals). Note the average single exponential decay function fitting curve in black.

(**H**) Heatmap snapshots of time-dependent spatial ΔF/F responses of an iAChSnFR expressing entorhinal stellate cell in response to local electrical stimuli in the normal bath solution and bath solution containing 1 μM TTX.

(**I**) Heatmap displays of three-dimensional spatiotemporal ΔF/F profiling of the same iAChSnFR expressing entorhinal stellate cell in response to local electrical stimuli in the normal bath solution and bath solution containing TTX. Note fluorescence ΔF/F responses with higher noise when imaged at ~120 nm/pixel resolution (with 60x objective) in **H-I** and one isolated release site indicated by pink arrow in **I**.

(**J**) Plot of relative maximal ΔF/F of each pixel against its distance to the pixel with largest maximal ΔF/F at the isolated release site indicated by pink arrow in **I**. Fitting the data points in this plot with a single exponential decay function (pink line) yields an estimated ACh spread length constant of 1.03 μm.

(**K**) Summary plot of volume spread length constants obtained from putative single release sites and the average ACh spread length constant of 1.06±0.09 μm for cholinergic transmission at entorhinal stellate neurons (n = 11 from 7 neurons from 4 animals). Note the average single exponential decay function fitting curve in black.

(**L**) Values of peak ΔF/F responses measured in the normal ACSF bath solution and ACSF containing TTX (Control: 100.0±5.0%; TTX: 22.2±5.2%; n = 11 from 4 animals; Z = −3.059, p = 0.002), or 0 mM Ca^{2}+/10 mM Mg^{2}+ ACSF (Control: 100.0±8.4%; 0 mM Ca^{2}+/10 mM Mg^{2+}: 1.3±2.3%; n = 10 neurons from 5 animals; Z = −2.803, p = 0.005). Large gray dots indicate average responses and asterisks indicate $p < 0.05$ (Wilcoxon Rank Sum tests).

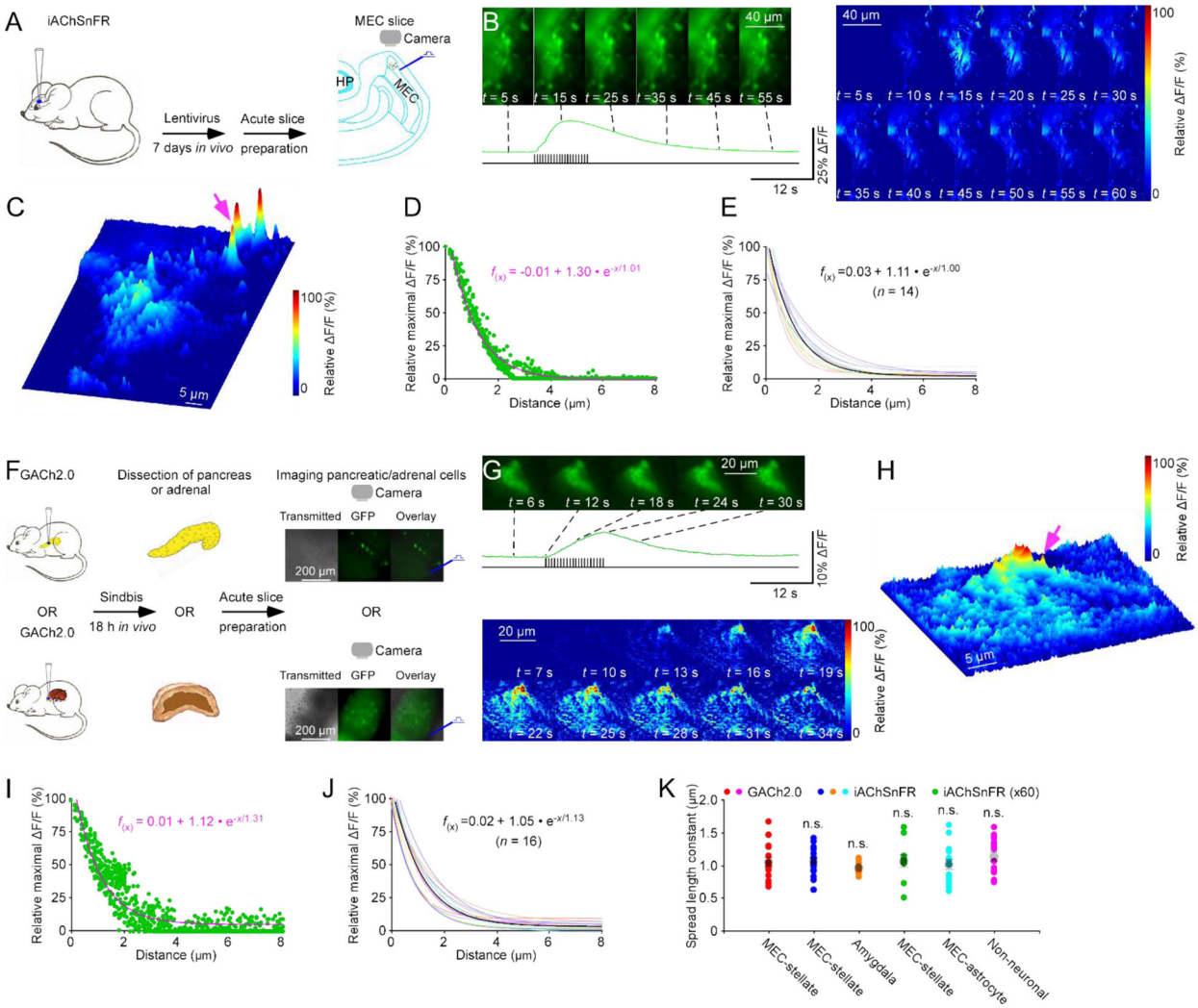

Figure 3. ACh sensors spatiotemporally profile cholinergic transmission at non-neuronal cells.

(**A**) Schematic drawing of the design of stimulation-imaging experiments with iAChSnFR in acute mouse MEC slices. HP: Hippocampus; MEC: Medial entorhinal cortex.

(**B-C**) Snapshots of fluorescence ΔF/F responses (**B** left panel), heatmap displays of time-dependent spatial ΔF/F responses (**B** right panel) and three-dimensional spatiotemporal ΔF/F profiling (**C**) of distal processes of an iAChSnFR expressing entorhinal astrocyte in response to local electrical stimuli. Note one isolated release site indicated by pink arrow in **C**. Note that the astrocytic cell body, localized below the image, was trimmed to highlight the responses at distal processes.

(**D**) Plot of relative maximal ΔF/F of each pixel against its distance to the pixel with largest maximum ΔF/F at the isolated release site indicated by pink arrow in **C**. Fitting the data points in this plot with a single exponential decay function (pink line) yields an estimated ACh spread length constant of 1.01 μm.

(**E**) Summary plot of volume spread length constants obtained from putative single release sites and the average volume spread length constant of 1.00±0.08 μm for cholinergic

transmission at entorhinal astrocytes (n = 14 from 8 neurons from 6 animals). Note the average single exponential decay function fitting curve in black.

(**F**) Schematic drawing of the design of stimulation-imaging experiments with GACh2.0 using an *in vivo* viral expression and *in vitro* mouse pancreatic and adrenal slice preparations. Inserts show transmitted light (left), fluorescence microscopic (middle) and overlay (right) images of GACh2.0 expressing pancreatic and adrenal cells.

(**G-H**) Heatmap snapshots of fluorescence ΔF/F responses (**G** upper panel), time-dependent spatial ΔF/F responses (**G** lower panel) and three-dimensional spatiotemporal ΔF/F profiling (**H**) of a GACh2.0 expressing pancreatic cell in response to local electrical stimuli. Note one isolated release site indicated by pink arrow in **H**.

(**I**) Plot of relative maximal ΔF/F of each pixel against its distance to the pixel with largest maximum ΔF/F at the isolated release site indicated by pink arrow in **H**. Fitting the data points in this plot with a single exponential decay function (pink line) yields an estimated ACh spread length constant of 1.31 μm.

(**J**) Summary plot of spread length constants obtained from putative single release sites and the average volume spread length constant of 1.13±0.07 μm for cholinergic transmission at the pancreatic and adrenal cells (n = 16 from 8 neurons from 8 animals). Note the average single exponential decay function fitting curve in black.

(**K**) Values for transmitter ACh spread length constants obtained with iAChSnFR at entorhinal stellate neurons (U = 115.0, p = 0.859; see data in Fig 2F), iAChSnFR under 60x objective at entorhinal stellate neurons (U = 74.0, p = 0.505; see data in Fig 2K), iAChSnFR at amygdalar neurons (0.96±0.02 pm; n = 12 from 4 neurons from 4 animals; U = 121.0, p = 0.225), iAChSnFR at entorhinal astrocytes (U = 124.0, p = 0.633; see data in Fig 3E), GACh2.0 at pancreatic and adrenal cells (U = 148.0, p = 0.462; see data in Fig 3J) compared to that obtained with GACh2.0 entorhinal stellate neurons (Mann-Whitney Rank Sum tests; see data in Fig 1F).

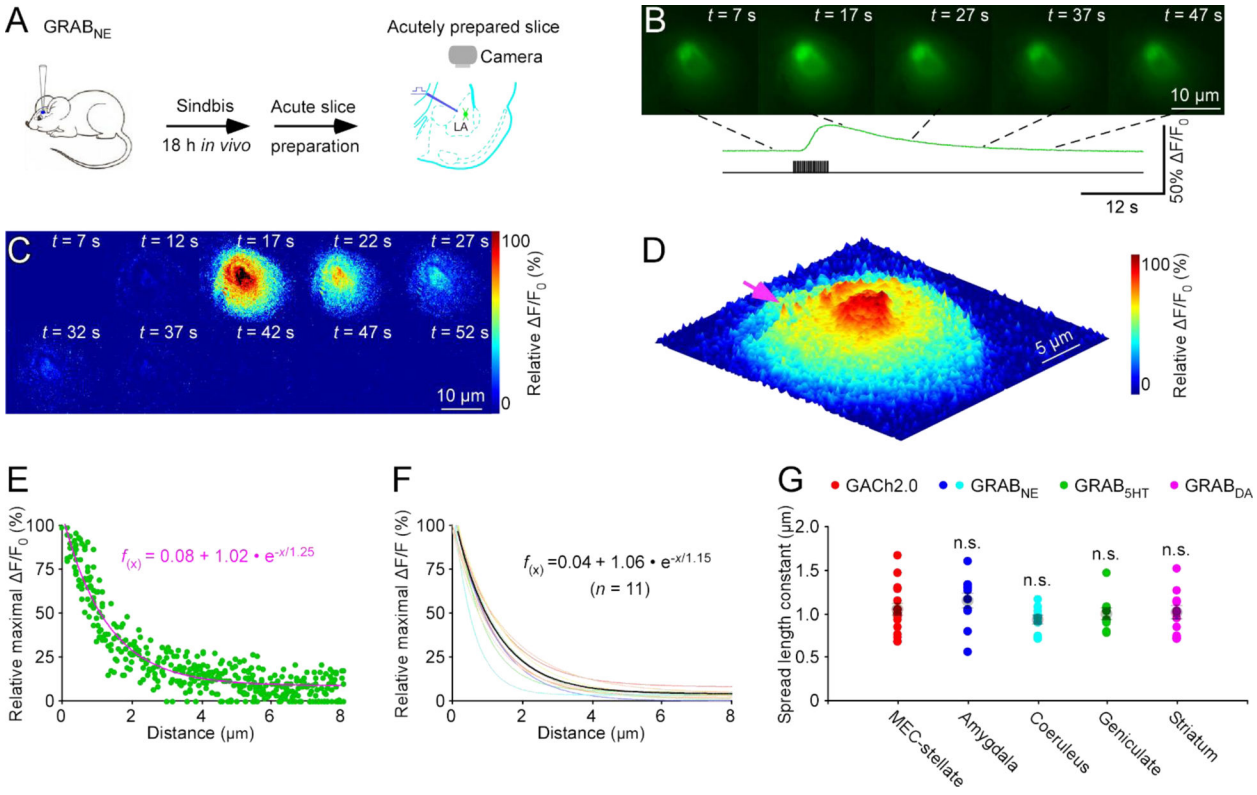

Figure 4. GRABNEim spatiotemporally profiles adrenergic transmission at amygdalar neurons.

(**A**) Schematic drawing of the design of stimulation-imaging experiments in acute mouse amygdalar slices. LA: Lateral amygdala.

(**B-D**) Snapshots of fluorescence ΔF/F responses (**B**), heatmap displays of time-dependent spatial ΔF/F responses (**C**) and three-dimensional spatiotemporal ΔF/F profiling (**D**) of a GRAB$_{NE1m}$ expressing amygdalar neuron to local electrical stimuli. Note one isolated release site indicated by pink arrow in **D**.

(**E**) Plot of relative maximal ΔF/F of each pixel against its distance to the pixel with largest maximum ΔF/F at the isolated release site indicated by pink arrow in **D**. Fitting the data points in this plot with a single exponential decay function (pink line) yields an estimated NE spread length constant of 1.25 μm.

(**F**) Summary plot of volume spread length constants obtained from putative single release sites and the average NE spread length constant of 1.15±0.09 μm for adrenergic transmission at amygdalar neurons (n = 11 from 5 neurons from 5 animals). Note the average single exponential decay function fitting curve in black.

(**G**) Values for monoaminergic transmitter spread length constants obtained with NE sensor at amygdalar neurons (U = 60.0, p = 0.175; see data in Fig 3E), and coerulear neurons (0.92±0.02 μm; n = 11 from 6 neurons from 6 animals; U = 113.0, p = 0.227), 5HT sensor at geniculate neurons (0.99±0.02 μm; n = 10 from 7 neurons from 3 animals; U = 88.0, p = 0.693), DA sensor at striatal neurons (1.00±0.07 μm; n = 11 from 6 neurons from 6 animals; U = 95.0, p = 0.748) compared to that obtained with GACh2.0 at entorhinal stellate neurons (Mann-Whitney Rank Sum tests; see data in Fig 1F).

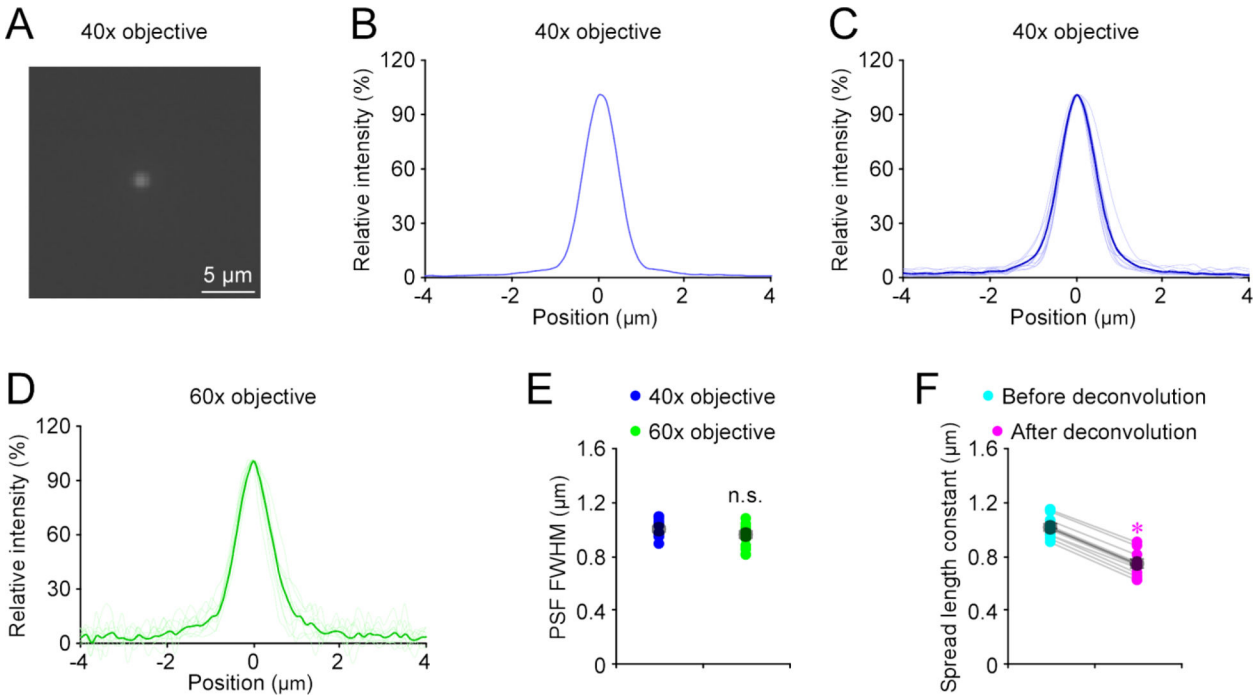

Figure 5. Point spread function of imaging setup.

(**A**) Fluorescence image of a 23-nm green GATTA bead under a 40x objective.

(**B**) Point-spread function (**PSF**) of the 23-nm green GATTA bead shown in (A) obtained under the 40x objective.

(**C**) Individual (light blue) and average (dark blue) PSFs of 23-nm green GATTA beads (n = 10) obtained under the 40x objective.

(**D**) Individual (light green) and average (dark green) PSFs of 23-nm green GATTA beads (n = 10) obtained under the 60x objective.

(**E**) Full width at half maximums (**FWHMs**) of PSFs of 23-nm green GATTA beads (n = 10) obtained under the 40x and 60x objectives (40x: 0.996±0.021 μm, n = 10; 60x: 0.950±0.027 μm, n = 10; U = 35.0, p = 0.273; Mann-Whitney Rank Sum test).

(**F**) Diffusion spread length constants before and after deconvolution with measured PSFs (Before: 1.01±0.03; After: 0.74±0.03; n = 10, Z = −2.803, p = 0.005). Asterisk indicates p < 0.05 (Wilcoxon Rank Sum test).